DISCLAIMER

This document was prepared as an account of work sponsored by the United States Government. While this document is believed to contain correct information, neither the United States Government nor any agency thereof, nor the Regents of the University of California, nor any of their employees, makes any warranty, express or implied, or assumes any legal responsibility for the accuracy, completeness, or usefulness of any information, apparatus, product, or process disclosed, or represents that its use would not infringe privately owned rights. Reference herein to any specific commercial product, process, or service by its trade name, trademark, manufacturer, or otherwise, does not necessarily constitute or imply its endorsement, recommendation, or favoring by the United States Government or any agency thereof, or the Regents of the University of California. The views and opinions of authors expressed herein do not necessarily state or reflect those of the United States Government or any agency thereof or the Regents of the University of California.

UCRL-1623
Unclassified-Physics Distribution

UNCLASSIFIED

UNIVERSITY OF CALIFORNIA

Radiation Laboratory

Contract No. W-7405-eng-48

THE POSITRON SPECTRUM FROM THE DECAY OF THE μ MESON

(Thesis)

Harmon William Hubbard

March 10, 1952

Berkeley, California

THE POSITRON SPECTRUM FROM THE DECAY OF THE μ MESON

Harmon William Hubbard

Radiation Laboratory, Department of Physics
University of California, Berkeley, California

March 10, 1952

INTRODUCTION

Two years after Yukawa's prediction of the existence of mesons, the light meson (subsequently named the μ meson) was found in cosmic radiation. Because the μ meson interacts only very weakly with atomic nuclei, it could not be the particle necessary for confirmation of Yukawa's ideas. It was later found that the μ meson results from the decay of a heavier particle of very short lifetime[1] this particle was named the π meson. It was first produced artificially at the Berkeley cyclotron[2]. The decay follows the scheme $\pi \rightarrow \mu + \nu$ (neutrino) with a mean life[3,4,5] of 2.5×10^{-8} sec. The μ meson is also radioactive, following the decay $\mu^{\pm} \rightarrow e^{\pm}$ + neutral particles, with a mean life[6,7,8,9] of 2.15×10^{-6} seconds. Many cloud chamber measurements of the energy of the decay electron or positron made it apparent that the decay electron did not have a unique energy, hence a three particle decay was assumed. That the electrons are given off with a spectrum of energies was shown conclusively by Steinberger[10]. The first attempt to measure the shape of the spectrum[11] showed that the neutral particles involved in the decay are of very small mass, comparable to the electron mass. More recently the spectrum has received additional attention,[12,13,14] but the results are somewhat contradictory.

The shape of the spectrum of μ meson decay electrons is of importance in making a correlation with ordinary β decay and in deciding the question of the feasibility of universal type of interaction between fermions. Further discussion of the theory is given in a following section.

METHOD

The 340 Mev external proton beam from the Berkeley 184-inch synchrocyclotron was used to produce a π^+ meson beam.[15] The protons were allowed to fall on a 2 inch thick polyethylene target situated between the pole pieces of a steering magnet. The reaction $p+p \rightarrow \pi^+ + d$ gives a yield of π^+ mesons which has a sharp peak in the π meson energy at about 65 Mev. The 2 inch target degrades the energy to 55 Mev with a width at half maximum of 4 Mev.[16,17,18] The magnet separated the resulting meson flux from the main proton beam and directed the nearly mono-energetic mesons through a hole made in the concrete shielding which surrounds the external beam port at the cyclotron. A cloud chamber was located just outside this hole in the shielding and the meson beam entered it. This experimental arrangement is diagrammed in Fig. 1.

The cloud chamber contained several thin carbon plates, and occasionally a π meson was slowed down and stopped in one of these plates. When this happened, the $\pi - \mu$ decay occurred in the carbon, and since the μ meson has a range of 0.8 mm of carbon when the π meson decays at rest, the μ meson did not normally emerge from the carbon plate, but decayed while in the carbon. About one half of the π mesons decay in flight before reaching the cloud chamber, so that the meson beam contains a small number of μ mesons which may be stopped, and decay in one of the carbon plates. In either case the decay positron from the μ meson then emerged from the plate into the gas of the cloud chamber. The identification of the μ decay

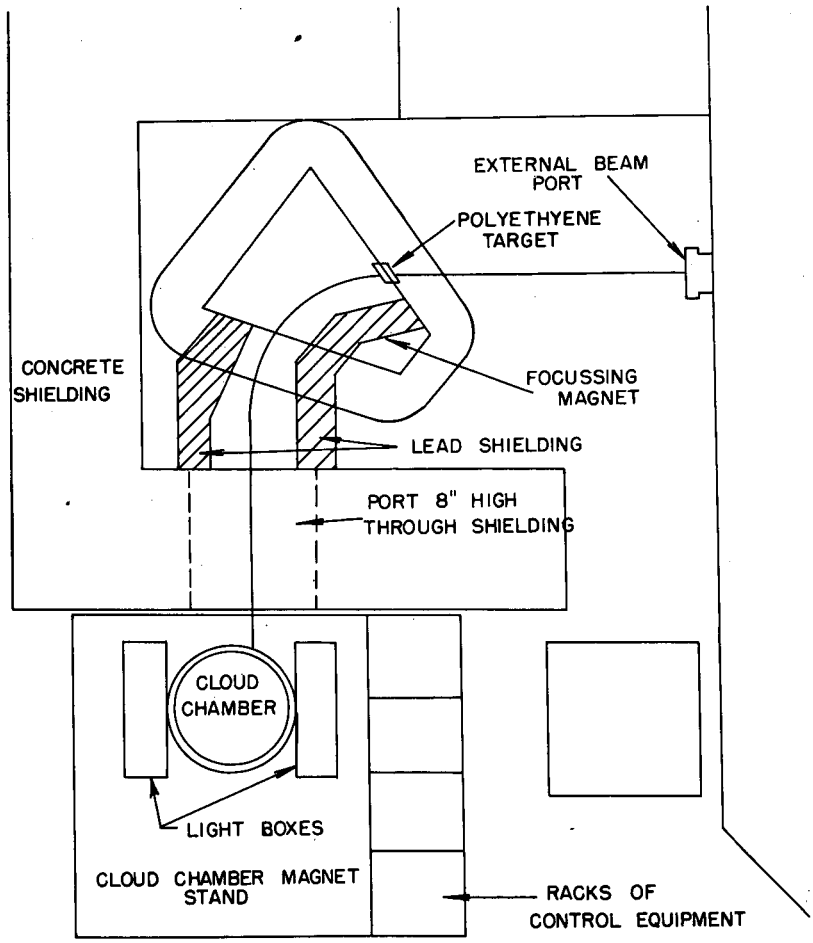

FIG 1

MU3260

190531

Fig. 1

Experimental setup used for taking the pictures.

positrons therefore was made contingent on finding the conjunction of a heavily ionized meson track and a lightly ionized positron track at some point on one of the plates. There were, of course, a few decays which occurred in the gas. That the identification is easy and definite will be made evident on examination of the photographs included in Appendix B. The probability of a random conjunction of π meson track and positron in the right energy range is exceedingly small.

The pictures were taken at a rate of one every 55 seconds. When the chamber was just fully expanded the ion source of the cyclotron was pulsed once, and the oscillator turned on for an appropriate interval to accelerate the protons to 340 Mev. The meson beam came through the cloud chamber. About 0.03 seconds after the arrival of the mesons, the lights were flashed and the picture taken. The magnetic field was kept at a steady value of 8200 gauss.

The energies of the positrons were measured from the photographs of the tracks on the film with the aid of a stereoscopic projector. This apparatus allows one to measure the radii of curvature of the positron tracks and the dip angle α, i.e. the angle between the plane most closely following the helix made by the track and the direction of the magnetic field. Knowing the radius of curvature ρ and dip angle one can calculate momentum of the particle from $cp = H\rho \sin \alpha$. The energy is obtained from the momentum measurement from the relation $cp = E$. This relation holds for $m_e c/p \ll 1$, which is the case for the entire region of interest. m_e = electron rest mass = 0.51 Mev.

The Experimental Equipment

The cloud chamber[19] is an expansion type, called a pantograph chamber because the bottom plate of the chamber is kept level during expansion by means of steel arms arranged in a way similar to a pantograph. This moving plate is covered with a sheet of rubber which extends over the edges of the plate and is clamped between the rim of the steel bottom and the side-wall of the cloud chamber which is a 1/2 inch thick lucite cylinder 3-1/2 inches high. The top glass is a circular, one inch thick piece of tempered plate glass with a beveled edge to accomodate the top ring which is tightened down by means of bolts which screw into the bottom plate. The useful depth of the cloud chamber is 2-1/2 inches, and the inside diameter is 22 inches.

The bottom of the chamber was coated with gelatin dyed black with a clothing dye. This procedure provided a glossy black surface giving very little diffuse reflection, and was therefore a good surface against which to photograph tracks strongly illuminated from the sides. The gelatin also provided the water vapor for the operation of the cloud chamber. The gelatin was made very thick, and was poured onto the bottom while hot enough to be liquid. A little copper sulfate mixed with it helped retard the formation of molds.

A clearing field of 50 to 100 volts was applied between the gelatin on the bottom and a very thin soap film on the under side of the top glass. The soap film was applied by hand rubbing until the glass appeared perfectly clear. Electrical contact with the soap film was made

by means of an aquadag ring painted on the top glass and contact with this was made with a thin foil inserted between the top gasket and the lucite cylinder. During operation the clearing field was turned off as the chamber began expansion, and turned on again after the lights had flashed. This was done to avoid distortion of the tracks in the electrostatic field.

Inside the cloud chamber, mounted in slots in the lucite cylinder, were several 3/16 inch thick (0.8 gm/cm^2) carbon plates extending across the chamber. These were coated with 0.002 inch aluminum foil to insure adequate lighting of all parts of the chamber. Two plates were used in the chamber, 4-1/2 inches apart, symmetrically spaced about the center. For the second run, four carbon plates were used; one at the center, one 3 inches in front of it (toward the meson beam), and two spaced at 3 inch intervals in back of it (away from the meson beam). For the second and third runs the cloud chamber also contained a 1/2 inch thick copper plate placed 3 inches in front (toward the beam) of the first carbon plate for the purpose of slowing down the mesons so that they had a possibility of stopping in a carbon plate. (μ meson decay positrons from a 1/2 inch copper plate cannot be used because of the large radiation straggling). During the first runs the copper absorber was placed outside the cloud chamber, but this proved undesirable because the large curvature of the slowed down mesons in the fringing field from the magnet prevented many of them from hitting the carbon plates and thereby very considerably reduced the number of desired events.

The cloud chamber magnet[19] is capable of producing a 21700 gauss pulsed field. During the runs for the present work the field was maintained steadily at about 8200 gauss. The field over the region of the cloud chamber is very uniform, and accurate field plots have been made over the entire useful region with the cloud chamber in the magnet. The space between the pole pieces is kept at 19° C by means of a water circulating system including a heater, a refrigerator and an electronic control system which continuously checks and adjusts the temperature by turning on and off the refrigerator and heater when necessary. The circumference of the gap in which the chamber rests is insulated with thick pieces of felt. The chamber itself is securely bolted to the bottom pole piece in order to prevent any motion when the field is turned on and off. A diagram of the magnet with the cloud chamber in place is shown in Fig. 2.

The photographs were taken with a stereoscopic camera equipped with two Leitz f/2 Summitar lenses spaced 4-1/2 inches apart, used at f/5.6. The camera was mounted 27-1/2 inches above the top glass of the cloud chamber. A third lens on the side opposite the stereoscopic pair photographed an ammeter in series with the magnet and a number counter. Eastman Orthochromatic Linagraph film was used.

The light sources used were two General Electric FT422 flash tubes, backed with aluminum foil as a reflector. Each tube was wrapped with 5 mil tungsten wire which served as a tickler to initiate the discharge. A capacitance of 1024 microfarads charged to 1600 volts was then discharged through each tube.

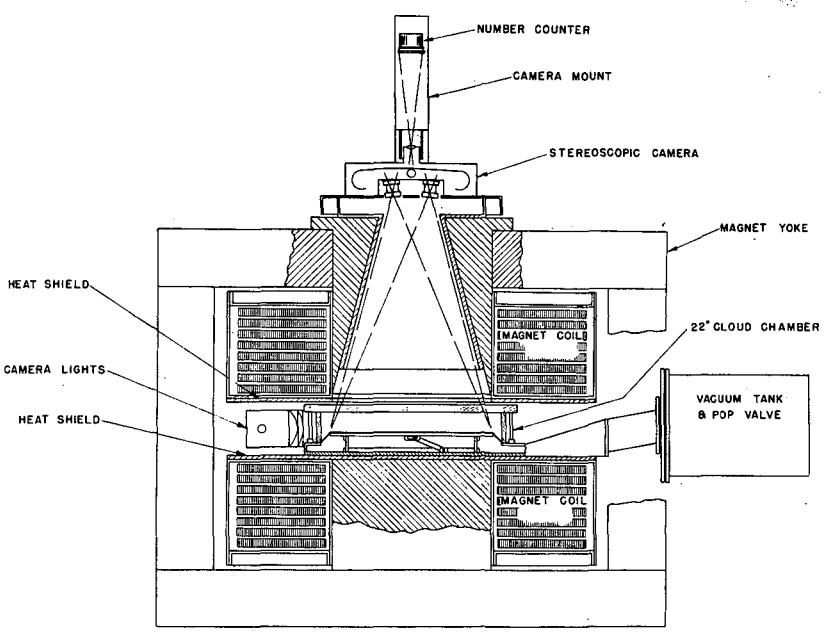

FIGURE 2

22 CLOUD CHAMBER ASSEMBLY

Fig. 2

Magnet with the cloud chamber in place.

Projection of the photographs is done through the camera lenses themselves. A diagram of the projector[20] is shown in Fig. 3. The projector essentially accomplishes an optical reconstruction of the cloud chamber interior at full size. Measurements were taken from the movable ground glass screen, the height and angle of which, for conjunction of the two stereoscopic images, measured the distance of the track from the cloud chamber bottom and the dip angle of the track. The radius measurements were taken from the image of the track on the ground glass screen by matching this image to the arc of a circle of known radius scratched on a thin lucite plate.

Accuracy and Limitations of the Measurements

The energy measurements have been carried out twice by different observers. This provided a check on the consistency of the measurements. Fig. 4 shows a plot of the number of tracks as ordinate and the amount by which two measurements of the same track differ from their mean as abcissa. This shows that on the average, measurements can be made to within ± 1.3 Mev. For the range of interest the radii of curvature are such that, with the 8000 gauss field used, the reproducibility of the measurements is very nearly independent of the energy of the electron.

The ionization loss per centimeter path of electrons from 5 to 55 Mev is practically constant. The carbon traversed by the positrons was measured for 104 cases by projecting the electron track back to its juncture with the meson track. (The μ meson has a range of 0.8 mm in carbon). The plates are 4.76 mm thick (3/16 inch) and the average distance traversed

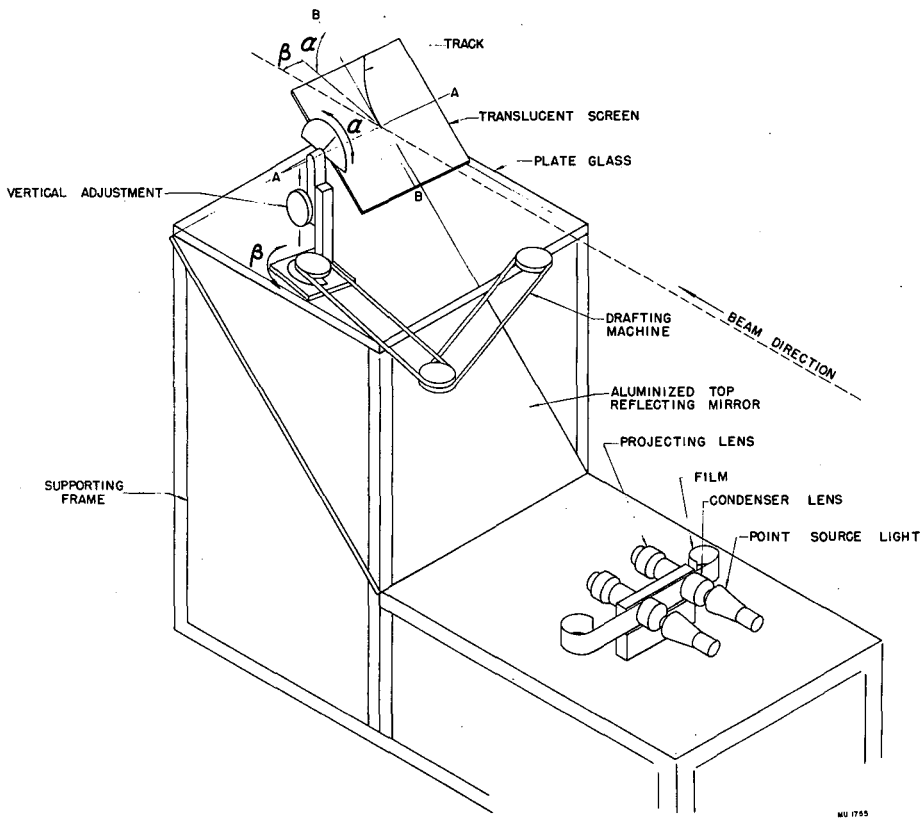

Fig. 3

Schematic diagram of the apparatus used for projection of the photographs.

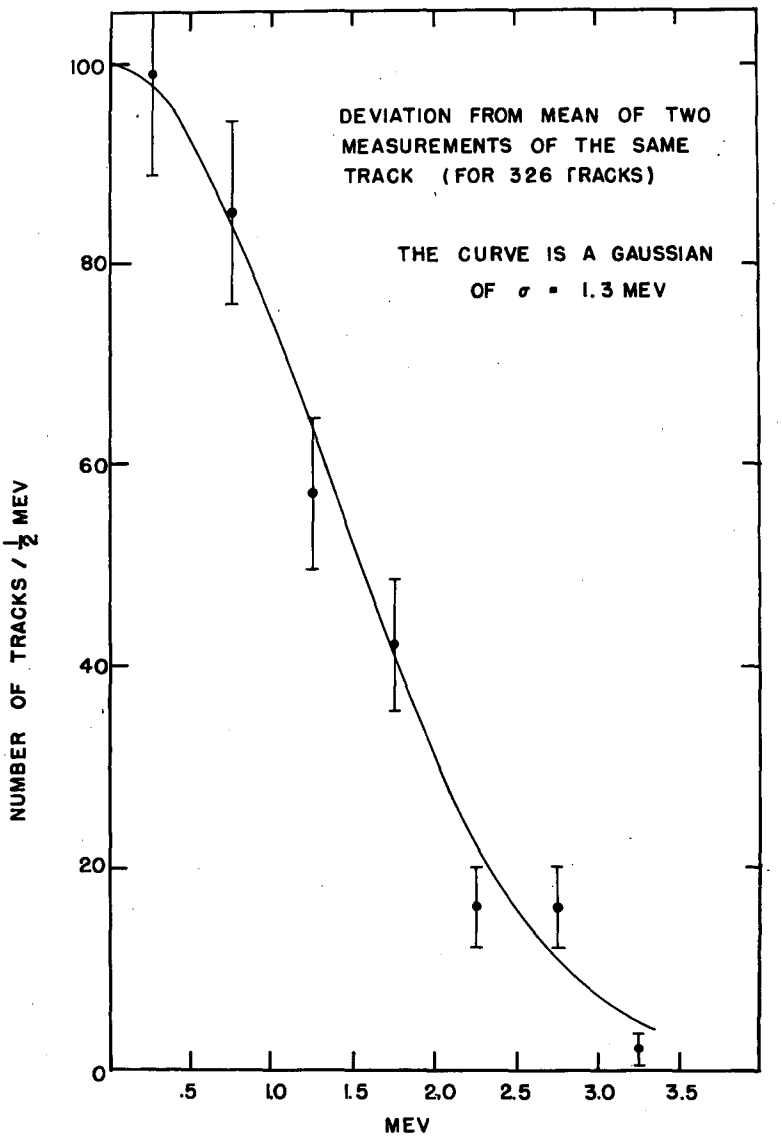

FIG. 4 MU 3264

Fig. 4

This curve is an indication of the consistency obtained on re measurement of 326 tracks by a second observer.

is 5.9 mm. For this distance the loss by ionization varies on the average from 1.8 Mev at 5 Mev to 2 Mev at 55 Mev. The curves used were corrected for the Fermi effect.

In taking account of the energy lost by radiation, the positron energies were corrected for the average loss in traversing 5.9 mm of carbon. It is clear that this procedure is justified if one considers that 3/16 inches of carbon (density 1.75 gm/cm^3) amounts to only 0.02 radiation lengths. The maximum r.m.s. straggling is about 0.5 Mev, and the average loss is about 1 Mev.

The uncertainty in radius of curvature expected from scattering in argon gas at 1-1/4 atmospheres pressure was calculated on the basis of the theory of multiple small angle scattering developed by Williams and Bethe[21]. The calculation makes use of the r.m.s. scattering angle and therefore yields an average radius of curvature due to scattering. The expected radius due to scattering depends on the length of track available for measurement. The magnitude of the scattering error is given in Table 1 for an 8000 gauss field. The shortest tracks measured were 6 cm long.

There are two effects which tend to emphasize high energy measurements. The first of these is that any random spurious curvatures superimposed on the curvatures of tracks due to the field tends to give a high value for the energy of the particle. This can be seen as follows.

Let the actual curvature of a track be $1/r$ and the superimposed one $1/r'$, then the measured curvature lies in the interval between $1/r + 1/r'$ and $1/r - 1/r'$. Then the radius lies between the reciprocals, i.e. between $r(1 + r/r')^{-1}$ and $r(1 - r/r')^{-1}$. The center of the interval

with these numbers as end points lies at $r/2\left[\frac{1}{1 + r/r'} + \frac{1}{1 - r/r'}\right] =$

$\frac{r}{1 - \frac{r^2}{r'^2}} > r$, and since on the average the measured <u>radius</u> is most likely to lie at the center of this interval, we will get consistently large measured values of r on the average due to any random spurious curvature such as scattering or turbulence. This effect is smaller for small r.

The second reason for expecting high energies to be overemphasized rests on the fact that since the positrons were observed emerging from the surface of a plate in a magnetic field, the observable solid angle available to positrons in the gas of the cloud chamber decreases with their energy because they curve back into the plate so that they cannot be seen, and since the positron is not emitted preferentially in any one direction the ratio of the number of tracks observed at, say, 50 Mev to the number at 15 Mev will be higher than the ratio of the numbers produced in the plates. We believe this effect has been eliminated by the device of discarding all tracks which make an initial angle with the surface of the plate of less than 30 degrees in a plane perpendicular to the field. None of the tracks below 10 Mev lie in this interval. Since we discard none of these lowest energy tracks, the numbers of tracks of various energies should be represented in their correct proportion because of the variation of the effect with energy mentioned above. Tracks having dip angles α greater than 60 degrees have also been excluded because the

error in determining the dip angle, though approximately constant for most dip angles, increases at large α and the corrections vary as the reciprocal of $\cos \alpha$.

During the experiment, pictures were taken periodically in the absence of a magnetic field. If tracks are observed due to particles of high enough energy so that gas scattering is negligible, any curvature of these "control" tracks can be ascribed to a turbulent motion of the gas in the cloud chamber. 100 such control tracks were carefully measured with the aid of a precision travelling microscope. The curvatures were measured by plotting the shape of the track on a scale enlarged in the direction of the sagitta so that it could be estimated more accurately. The distribution of these turbulence curvatures is given in Fig. 5. Curvatures of both signs occurred with equal frequency and since the measured positron tracks also have curvatures of both signs with equal frequency, a plot which does not distinguish signs of the turbulence curvatures is the correct one to use.

In order to find the energy resolution allowed by a given curvature distribution due to random effect, let us call the random curvatures C_t and let the normalized distribution be $P(C_t)$. i.e. $\int_{-\infty}^{\infty} P(C_t)dC_t = 1$. Then $P(C_t)$ is the probability that an actual curvature C is measured as a curvature $C + C_t$ in the interval from C to C + dC. On changing to a distribution in radius of curvature r, $C = 1/r$, $P(1/r)\, dr/r^2$ is the probability that an actual radius r be measured as $(1/r \pm 1/r_t)^{-1}$ in the interval from r to r + dr. The energy E of the positrons is equal to ar

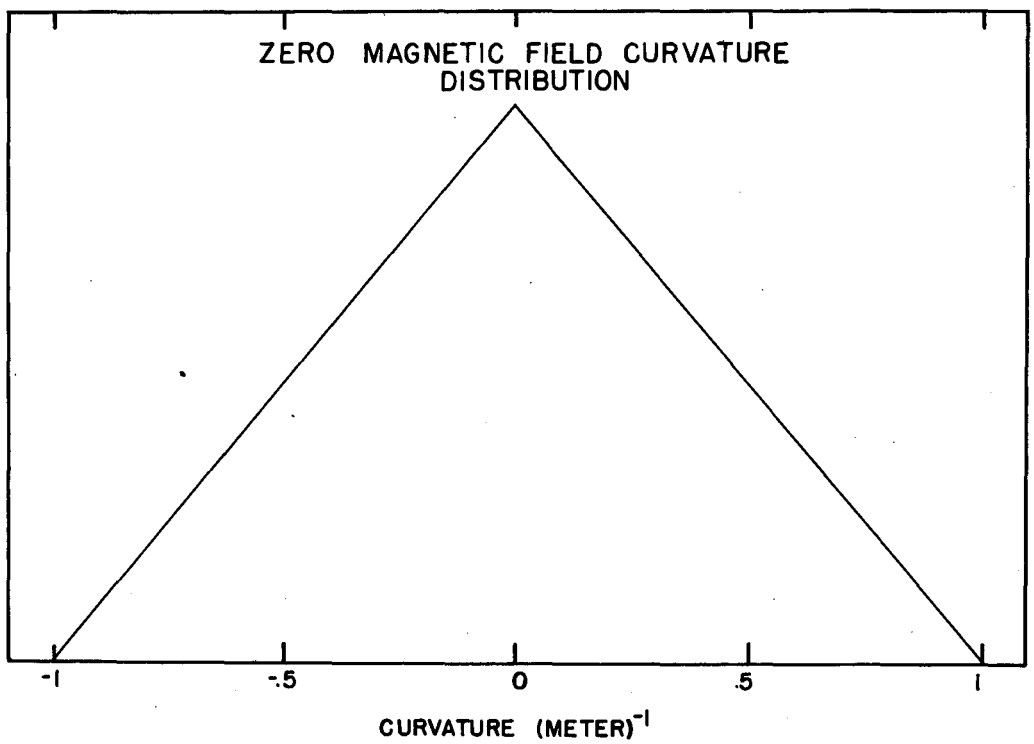

FIG. 5

MU 3261

Distribution of measured zero field curvatures from 100 tracks. The distribution is due to gas turbulence.

where a = 240 Mev meter^{-1} for an 8000 gauss field. Hence the probability per Mev that E be measured as $(1/E \pm 1/E_t)^{-1}$ as a function of E is

$$K\left[E,\ (1/E \pm 1/E_t)^{-1}\right] = a/E^2 \quad P(\pm\, a/E_t)$$

where $E_t = \begin{cases} a/C_t\ , & C_t > 0 \\ -a/C_t\ , & C_t < 0 \end{cases}$

Now let us replace E by $(1/E \pm 1/E_t)^{-1}$ and we have $K\left[(1/E \pm 1/E_t)^{-1}, E\right] = a\,(1/E \pm 1/E_t)^2\ P\,(\mp\, a/E_t) = E^2\ (1/E \pm 1/E_t)^2\ \ K\left[E, (1/E\ \ 1/E_T)^{-1}\right]$. If now one puts $E' = (1/E \pm 1/E_t)^{-1}$ there results $K(E', E) = (E/E')^2\ K(E, E')$. To find the effect of turbulence on a theoretical spectrum $f(E)$ we proceed as follows: $f(E')\ dE'\ K(E', E)\ dE$ is the probability that a μ meson decay electron from the energy interval dE' about E' be measured as lying in the interval dE about E. By considering contributions from all parts of the spectrum $f(E')$, we get the probability that any μ decay electron be measured as lying in the interval dE about E. This is just $F(E)\ dE = dE \int_0^{E_{max}} f(E')\ K\ (E', E)\ dE'$ and is the spectrum which would be measured if $f(E)$ were the correct theoretical spectrum. From the above considerations we can calculate K(E', E) for any pair of energies E', E, and can therefore calculate the measured spectrum to be expected from any theoretical spectrum $f(E)$. The "resolving power" K(E', E) which arises from the distribution of Fig. 5 is shown in Fig. 6. It is clear from this plot that turbulence of the gas is responsible for the major part of the uncertainty in the energy measurements.

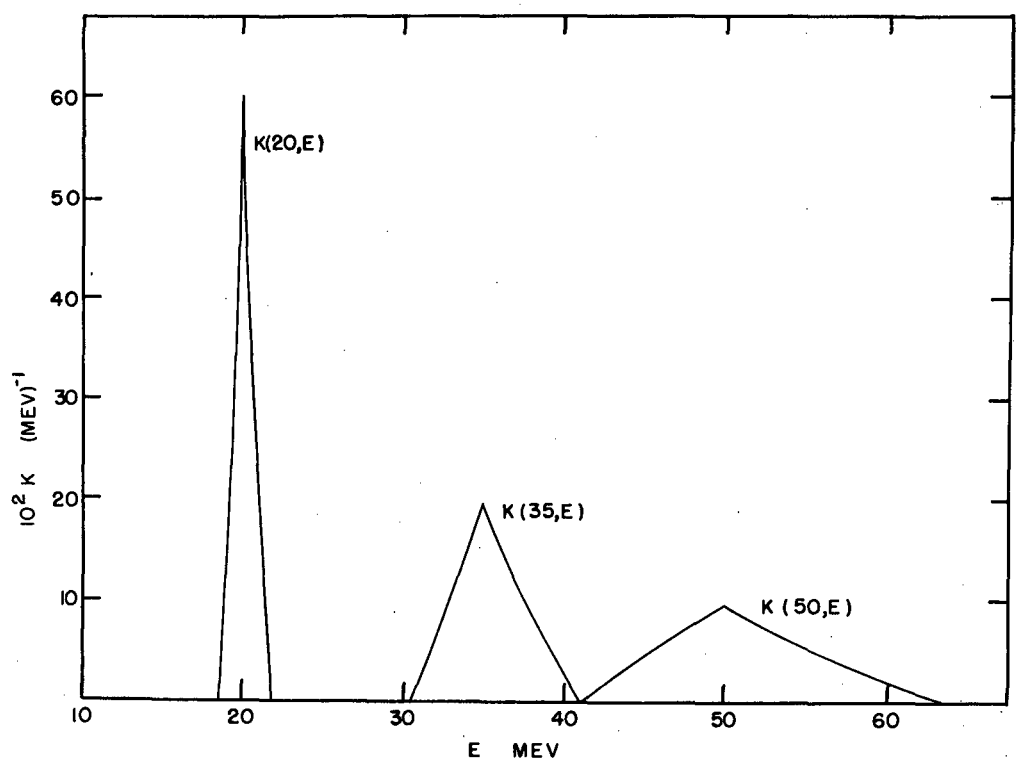

FIG. 6

MU 3262

These curves represent the resolving power of the cloud chamber for 20, 35, and 50 Mev. These are the spectra which would be measured if one shot monoenergetic beams of the above energies through the chamber.

Theory of the Decay Process

Theoretical discussions of the μ meson decay problem have been given by J. Tiomno and J. A. Wheeler[22] and by L. Michel[23]. Michel's treatment is more general and his results are more readily compared with experiment. Both treatments assume a spin of 1/2 for the μ meson and use Schrödinger perturbation theory to calculate the probability per second of decay as function of electron energy. The interaction energy responsible for the decay is in both cases taken as a direct interaction of the four fields of which the field particles are the μ meson, the electron or positron, and the two neutral particles. The interactions are the β decay interactions made up from Dirac's matrices. The interaction is therefore one of S = scalar, V = vector, T = Tensor, PV = pseudovector or PS = pseudoscalar, or a linear combination of any or all of these. Michel's treatment differs from that of Tiomno and Wheeler in that he considers a general linear combination of all five types of interaction.

The shape of the positron spectrum depends on the masses of the neutral particle emitted in the decay. It is shown in Appendix A, however, that the shape of the spectrum is influenced only in the immediate neighborhood of the maximum energy W, provided the neutral particle mass is small with respect to the positron energies of interest. Because this effect is not large enough to be observed in this experiment, we will consider the two neutral particles to be zero mass neutrinos, so that we will discuss only the decay $\mu \rightarrow e + 2\nu$. For this process laws of the conservation

of energy and momentum yield the maximum electron energy

$$W = \frac{M_\mu^2 - M_e^2}{2M_\mu} \approx \frac{M_\mu}{2},$$

where M_μ = mass of the μ meson, M_e = mass of the electron. We measure both masses and energies in energy units (corresponding to taking the speed of light c = 1), and therefore also momentum is measured in energy units. We will adhere to this convention. For $M_\mu = 210\ M_e$[24] one finds W = 53.6 Mev.

The calculation of the shape of the spectrum is made in the following way: The probability per unit time of a μ meson decay leaving the electron or positron in the energy interval dE is given by the standard formula from Schrödinger perturbation theory as

$$\frac{2\pi}{\hbar}\left|H\right|^2\left(\frac{dN}{dE_t}\right)_{E_t=M_\mu} dE$$

where E_t is the total energy available in the rest system of the μ meson, H is the interaction energy matrix element, and dN/dE_t is the total number of final states per unit total energy consistent with the decay electron having energy E.

After the decay the two neutrinos and the electrons are assumed to behave as free particles. Let V be the volume of the region in which the free particle wave functions are normalized, and let $\vec{p}$ be the electron momentum and $\vec{p_1}$, $\vec{p_2}$ the neutrino momenta, Since $\vec{p_2}$ may be

eliminated, the total number of states per unit energy for which the electron momentum makes angle θ with $\vec{p_1}$ is

$$\left.\frac{dN}{dE_t}\right|_{E_t=M_\mu} = \frac{V}{h^3}\, d\vec{p}\, \frac{V}{h^3} \left(\frac{d\vec{p_1}}{dE_t}\right)_{E_t = M_\mu} = \frac{8\pi^2 V^2}{h^6}\, p^2\, dp\, p_1^2 \left(\frac{\partial p_1}{\partial E_t}\right)_{E_t = M_\mu} \sin\theta\, d\theta$$

Conservation of momentum requires $\vec{p} + \vec{p_1} + \vec{p_2} = 0$ and conservation of energy requires $E_t = E + E_1 + E_2 = M_\mu$ and the momenta and energy are related by $E = p^2 + M_e^2$, $E_1 = p_1$, $E_2 = p_2$. On eliminating p_2 these equations yield $p_1 = \dfrac{M_\mu(W - E)}{M_\mu - E + p\cos\theta}$ where θ is the angle between $\vec{p_1}$ and $\vec{p}$, and

$$\left.\frac{\partial p_1}{\partial E_t}\right)_{E_t = M_\mu} = \frac{(M_\mu - E)\,(M_\mu - E + p\cos\theta) - M_\mu\,(W - E)}{(M_\mu - E + p\cos\theta)^2}$$

Since $p^2 = E^2 - M_e^2$ we may consider p_1 and $\left.\dfrac{\partial p_1}{\partial E_t}\right)_{E_t = M_\mu}$ as functions of p and $\cos\theta$. Let us call $p_1^2 \left.\dfrac{\partial p_1}{\partial E_t}\right)_{E_t = M_\mu} = \phi\,(p, \cos\theta)$. Then the probability per unit time of a μ meson decay leaving the electron with momentum p in dp and for which the electron momentum and neutrino number 1 momentum make an angle θ is

$$\frac{V^2\, 16\pi^3}{\hbar\, h^6}\, p^2\, dp\, \left|H\right|^2 \phi(p, \cos\theta)\, \sin\theta d\theta.$$

Hence the probability per unit time of leaving the electron with momentum p in dp is just

$$P(p)dp = \frac{V^2\, 16\,\pi^3}{\hbar\, h^6}\, p^2\, dp \int_0^\pi \left|H\right|^2 \phi(p, \cos\theta)\, \sin\theta\, d\theta \text{ which}$$

gives the energy spectrum. H is in general a function of both p and θ.

On making this calculation with H an arbitrary linear combination of all five of the β decay interaction Michel finds a result which reduces on putting $p = E$, $(M_e \ll E)$ to

$$P(E) = \frac{1}{\tau} \frac{12 E^2}{W^4} \left[(W-E) + 2/9\, \rho\, (4E - 3W)\right]$$

where τ is the μ meson mean life. (The lifetime enters because of the requirement $\int_0^W P(E)\, dE = 1/\tau$.) ρ is a parameter, $(0 \leq \rho \leq 1)$ which is determined by the amounts of the interactions present, provided certain other specifications are made. $f(E) = \tau P(E)$ is the probability per Mev of a μ meson decay leaving an electron of energy E in dE. Plots of the function $f(E)$ for several values of ρ are given in Fig. 7. Note that $f(W)$ is proportional to ρ, and that $f(3/4\, W) = f(40.2 \text{ Mev})$ is independent of ρ so that the theory predicts the measured spectrum (properly normalized so that $\int_0^W f(E)dE = 1$) must pass through the point $f = 3.16 \times 10^{-2}\ (\text{Mev})^{-1}$ at $E = 40.2$ Mev for any kind of interaction.

Since the amounts of the various interactions causing the μ meson decay enter into the theoretical spectrum only through the parameter ρ, the question arises to what extent an experimental determination of the number ρ determines the amounts of the different interactions which are present to cause the actual decay process. To answer this question consider that in order to form the matrix elements of the interaction energy the four fields μ, e, ν_1, ν_2 are arranged into two pairs, with the same interaction between each pair. (One of S = Scalar, V = vector, T = Tensor, PS = pseudoscalar and PV = pseudovector, or a linear combination of any or all of these.) The interaction energy

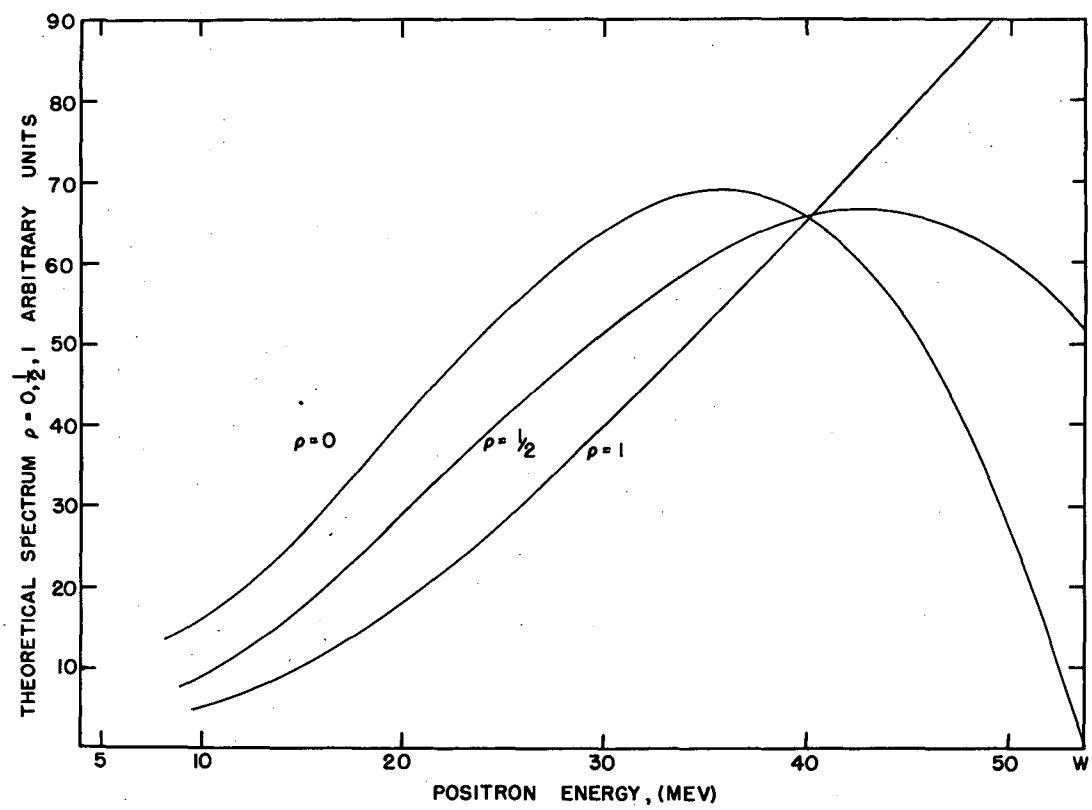

FIG. 7

MU 3263

Theoretical spectra for zero mass neutral particles. The parameter ρ is determined by the type of coupling, the order of particles in the hamiltonian, and by whether the neutrinos are taken to be identical or not.

between the four particles cannot be influenced by an interchange of particles, so the interaction hamiltonian must remain invariant on a permutation of the particles. On such a permutation the interactions (S, V, T, PV, PS) have to undergo a linear substitution among themselves according to the five dimmensional respresentation of the four object permutation group induced in the five dimensional "space" of the five interactions by the permutation of the particles. In short, a permutation of the particles changes the amounts of the five kinds of interactions present, so that one must state the order of particles in the hamiltonian if he also wishes to state the amounts of the various kinds of interaction present. This situation is somewhat ameliorated by the fact that interchange of particle of a pair or of the order of the pairs themselves changes only the sign of some of the coupling constants, an interchange of a particles of one pair with a particle of the other pair being the only kind of permutation which makes a difference in the results. There are therefore only two cases to distinguish on this account, for example the orders (μe) $(\nu\nu)$ and $(\mu\nu)$ $(e\nu)$. Tiomno and Wheeler call the differences in order of the particles different "theories". There can be, of course, no physical difference. The only coupling independent of order is the Critchfield-Wigner interaction[25,26] S + PS - PV.

The second ambiguity arises because the neutrinos may be considered identical particles. If two of the four fields are identical, then there exist two relations between the five interactions for a <u>given</u> order, i.e. there are only three linearly independent interactions. The

cases for identical neutrinos must therefore be considered separately.

The values of ρ for the four different cases are listed in Table 2. The g's are the coupling constants giving the strengths of the various interactions indicated by a subscript. It can be seen that for any of the cases the Critchfield-Wigner coupling S + PS - PV yields $\rho = 1/2$.

RESULTS

The energy spectrum obtained from 405 tracks is plotted in Fig. 8. Statistical standard deviations are shown through the experimental points. The solid line curve is the theoretical curve for $\rho = 0.26$, and the dashed curve shows the effect of turbulence on the theoretical curve, calculated in the way explained above. The average energy is 34.2 ± 1 Mev. The most probable energy is about 40 Mev.

In order to plot the results as a differential energy spectrum, intervals of $\Delta E = 10$ Mev have been used. Let ΔN_i be the number of tracks in the ith interval. Then the spectrum will be normalized to unit area if we plot $1/N\ \Delta N_i/\Delta E_i$ as function of energy, where $N = 405$ is the total number of tracks. Plotted in this way, the numbers read from the curve give directly the probability of decay per Mev for a positron of the energy chosen. Both this scale and a scale for ΔN_i are shown in Fig. 8. Table 3 gives the number of tracks in each energy interval.

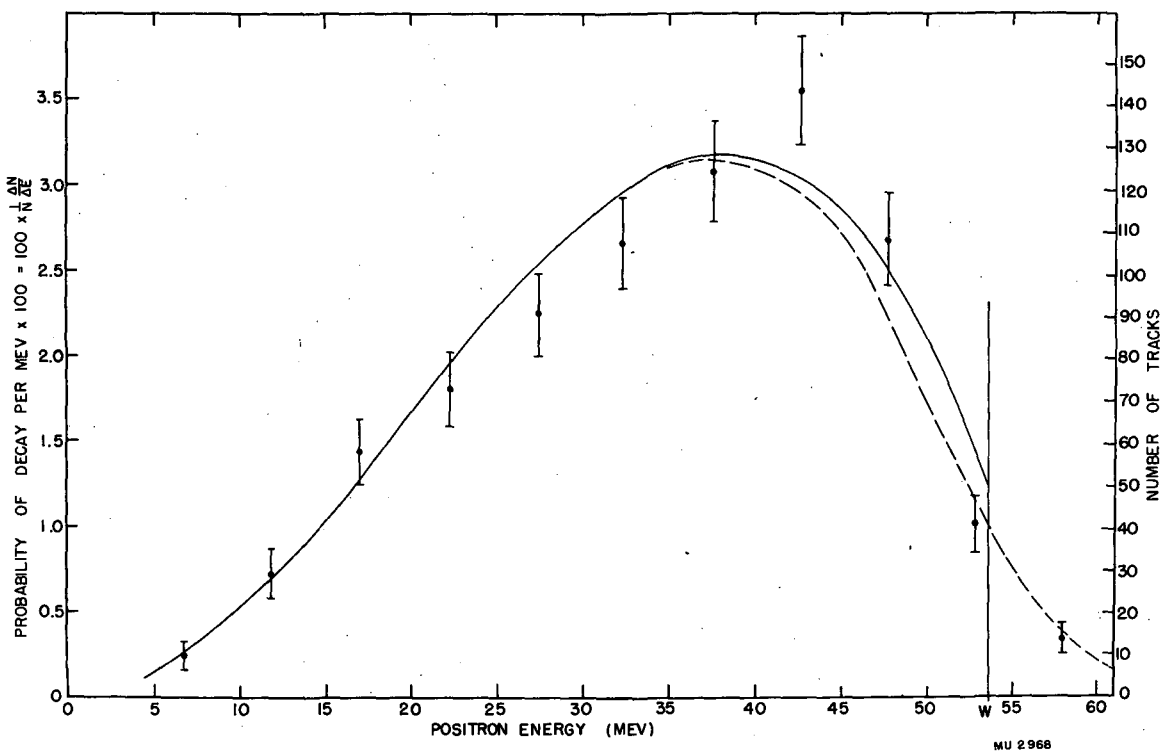

Fig. 8

Experimental results for 405 positron tracks. Standard deviation is shown for the experimental points. The solid curve is a theoretical curve for $\rho = 0.26$. The dashed curve shows the effect of the resolving power of Fig. 6 on the theoretical curve.

DISCUSSION

According to the theory, the only connection between the shape of the energy spectrum and the type of interaction between the particles which is responsible for the decay is given by the parameter ρ. Therefore, it is important to obtain as accurate a determination of this number as the experiment will allow. Perhaps the most accurate method is the following one.

From the form of the theoretical spectrum

$$f(E) = 12\ E^2/W^4 \left[(W - E) + 2/9\ \rho\,(4E - 3W)\right]$$

one notices that $f(E)/E^2$ is a linear function of E, so that if the experimental results are plotted as const. $1/E^2$ $1/N$ $\Delta N/\Delta E$ a straight line should result if the theory is correct. By choosing the constant properly one can make the intercept at E = W have the value ρ. For this case one plots $g(E) = 3/8\ W^3/E^2 f(E)$. Graphs of g(E) for various values of ρ are shown in Fig. 9. One notices that all the lines past through g = 9/8 at E = 3/4 W = 40.2 Mev. Hence one has a method at hand for determination of ρ which uses all of the data; namely one plots the experimental data as described, then draws a straight line through the point g = 9/8 at E = 3/4 W and adjusts the slope of the line to make a least squares fit to the experimental points. One can then read off the value of ρ from the intercept at E = W. In this way one obtains a value $\rho = 0.26 \pm 0.26$ from the data of Fig. 8. The data are shown plotted in this way in Fig. 10, the solid curve being drawn for $\rho = 0.26$ and the dotted curve showing the

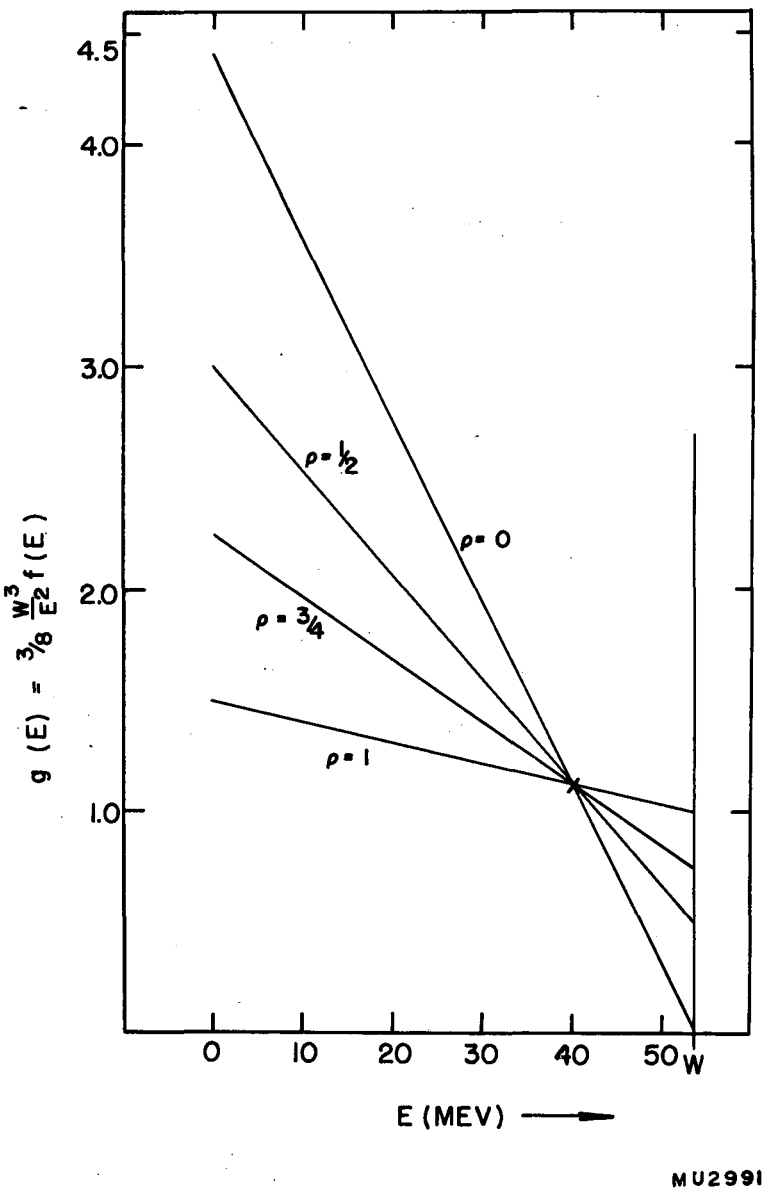

Fig. 9

Theoretical curves $g(E) = 3/8 \; W^3/E^2 \; f(E)$ where $f(E)$ is plotted in Fig. 7. The straight lines all pass through $g = 9/8$ at $E = 3/4 \; W = 40.2$ Mev, $g(W) = \rho$.

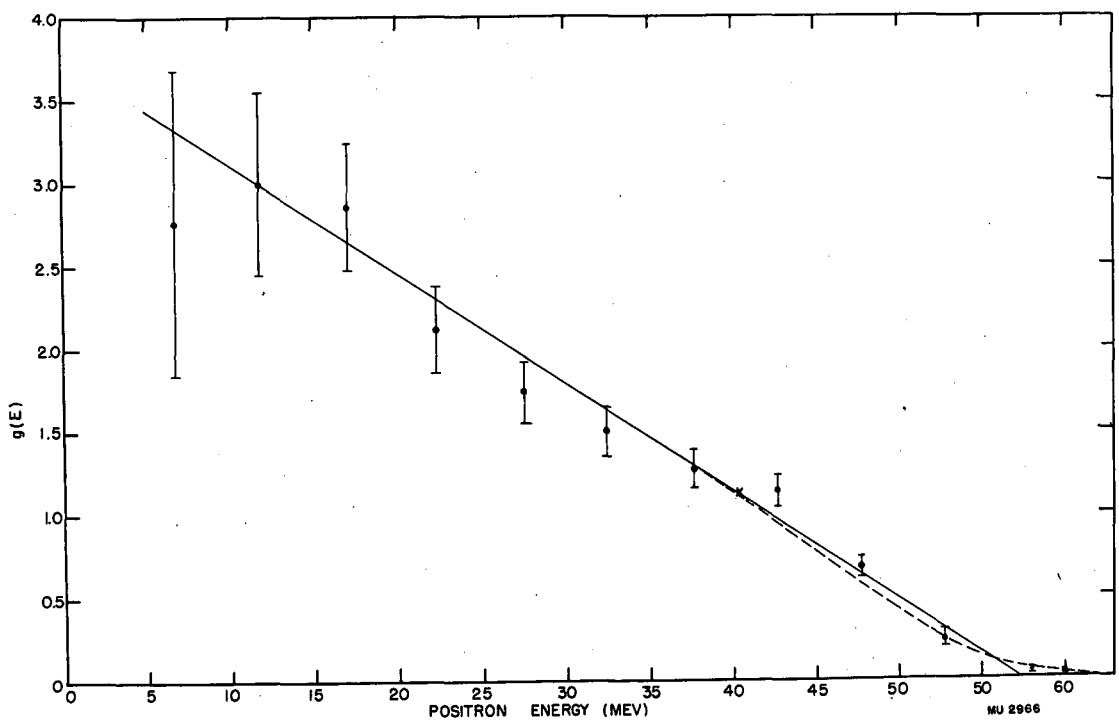

Fig. 10

Experimental results for 405 tracks on the straight line plot. Standard deviation is shown for the experimental points. The solid line is the theoretical curve for $\rho = 0.26$ and the dashed curve shows the effect of the resolving power of Fig. 6 on this curve. The point x marks the energy $E = 3/4\ W = 40.2$ Mev and $g = 9/8$, through which the measured curve must pass according to the theory.

effect of turbulence. This type of analysis applied to the data of other experimenters[12,13,14] does not yield a more accurate value of ρ but does make it evident that perhaps 1/2 is a reasonable upper limit to assign. If we exclude the value 1/2 we have excluded the Critchfield-Wigner interaction and although the data are not sufficient to decide definitely that $\rho<1/2$, it seems highly probable. The Critchfield-Wigner interaction is attractive as a possibility for both ordinary and μ meson β decay because of its symmetry properties mentioned above, but it appears it cannot explain the experimental μ decay β spectra.

In conclusion we would like to thank Professors W. K. H. Panofsky and J. Steinberger for suggesting the experiment, Mrs. A. Overhauser for reading many of the tracks, and particularly Mr. P. Moulthrop for valuable assistance throughout the course of the experiment. We wish to express our sincere gratitude to Professor Wilson M. Powell for his guidance, many helpful suggestions and valuable criticisms, and active interest throughout this work and for making available the facilities of the cloud chamber group at the University of California Radiation Laboratory.

TABLE 1

Positron Energy (Mev)	r.m.s. % uncertainty in radius due to scattering. Track length 5 cm	Track length 10 cm
10	2.64	1.87
20	2.98	2.11
30	3.12	2.20
40	3.29	2.32
50	3.31	2.37
60	3.44	2.43

TABLE 2

[S = Scalar, V = Vector, T = Tensor, PS = Pseudoscalar, PV = Pseudovector]

Order	Neutrinos	Tiomno-Wheeler Designation	ρ
(μe) $(\nu\nu)$	Distinguishable	Charge retention	$\dfrac{3(g_V^2 + 2g_T^2 + g_{PV}^2)}{g_S^2 + 4g_V^2 + 6g_T^2 + 4g_{PV}^2 + g_{PS}^2} \leq 1$
$(\mu\nu)$ $(e\nu)$	Distinguishable	Simple charge exchange	$\dfrac{3/4\ \left[(g_S - g_T)^2 + (g_T + g_{PS})^2 + 2(g_V + g_{PV})^2\right]}{g_S^2 + 4g_V^2 + 6g_T^2 + 4g_{PV}^2 + g_{PS}^2} \leq 1$
(μe) $(\nu\nu)$	Identical		$\dfrac{3g_{PV}^2}{g_S^2 + 4g_{PV}^2 + g_{PS}^2} \leq 3/4,$
$(\mu\nu)$ $(e\nu)$	Identical	Antisymmetric charge exchange	$\dfrac{3/2\ \left[g_S + g_{PS} - 2(g_V + g_{PV})\right]^2}{(g_S + 6g_T - g_{PS})^2 + 16(g_V - g_{PV})^2 + 2\ \left[g_S + g_{PS} - 2(g_V + g_{PV})\right]^2}$ is less than 3/4

TABLE 3

Number of Tracks ΔN as Function of E.

ΔE	0-10	5-15	10-20	15-25	20-30	25-35	30-40	35-45	40-50	45-55	50-60
ΔN	9	29	58	73	91	108	125	144	109	44	13

REFERENCES

1. C. M. G. Lattes, H. Muirhead, G.P.S. Occhialini and C. F. Powell, Nature 159, 694 (1947) and 160, 486 (1947).

2. E. Gardner and C. M. G. Lattes, Phys. Rev. 74, 1236 (1948).

3. O. Chamberlain, F. Mozeley, J. Steinberger and C. Wiegand, Phys. Rev. 79, 394 (1948).

4. M. Jakobson, A. Schulz, and J. Steinberger, Phys. Rev. 81, 894 (1951).

5. C. Wiegand, Phys. Rev. 83, 1985 (1951).

6. N. Nereson and B. Rossi, Phys. Rev. 64, 199 (1943).

7. M. Conversi and O. Piccioni, Phys. Rev. 70, 859 (1946).

8. H. K. Ticho, Phys. Rev. 74, 1337 (1948)

9. W. Bell and E. Hincks, Phys. Rev. 84, 1243 (1951).

10. J. Steinberger, Phys. Rev. 75, 1136 (1949)

11. R. B. Leighton, C. D. Anderson and A. J. Seriff, Phys. Rev. 75, 1432 (1949).

12. R. Sagane, W. Gardner and H. Hubbard, Phys. Rev. 82, 557 (1951).

13. H. Bramson and W. Havens, Phys. Rev. 83, 861 (1951).

14. A. Lagarrigue and C. Peyrou, Journal de Physique et du Radium (to be published).

15. C. Richman, M. Skinner, J. Merritt, and B. Youtz, Phys. Rev. 80, 800 (1950).

16. F. Cartwright, C. Richman, M. Whitehead and H. Wilcox, Phys. Rev. 78, 823(1950).

17. F. Crawford, K. Crowe and L. Stevenson, Phys. Rev. 82, 97 (1951).

18. M. Whitehead and C. Richman, UCRL-1530.

19. W. M. Powell, Rev. Sci. Inst. 20, 403 (1949).

20. K. Brueckner, W. Hartsough, E. Hayward and W. M. Powell, Phys. Rev. 75, 555 (1949).

21. H. A. Bethe, Phys. Rev. 70, 821 (1946).

22. J. Tiomno and J. A. Wheeler, Rev. Mod. Phys. 21, 144 (1949).

23. L. Michel, Proc. Phys. Soc. 63A, 514 (1950).

24. F. Smith, W. Barkas, A. S. Bishop, H. Bradner, and E. Gardner, Phys. Rev. 78, 86(1950).

25. L. Critchfield and E. Wigner, Phys. Rev. 60, 412 (1941).

26. L. Critchfield, Phys. Rev. 63, 417 (1943).

APPENDIX A

If one assumes one of the neutral particles to have a mass M different from zero, but small compared to the electron energies measured, then Michel's results for the spectrum can be written as

$$\frac{E^2\ (W-E)^2\ \left[(W-E)+\frac{3M^2}{2M_\mu}\right]}{\left[(W-E)\ +\ M^2/2M_\mu\right]^3}\left\{W(3a+b+c)-E\ (2a+2b+c)+\frac{2\ (W-E)^2}{\left[(W-E)+\frac{3M^2}{2M_\mu}\right]}\ (b+c)\right\}$$

where a, b, and c depend on the strengths of the interactions. This reduces to the above result for two neutrino decay if $W-E \gg M^2/2M_\mu$. Therefore the formula for the spectrum for zero mass neutral particles will hold for finite mass M also, except for a region of the order of $M^2/2M_\mu$ next to the maximum energy W. The maximum energy for this case is

$$W = \frac{M_\mu^2\ M_e^2 - M^2}{2M_\mu} \approx \frac{M_\mu}{2} - \frac{M^2}{2M_\mu}$$

so that in applying the zero mass formula where $W \approx M_\mu/2$ we need to allow an extra interval $M^2/2M_\mu$ down from the maximum, i.e. $W-E \gg M^2/M_\mu$. If $M = 20.2\ M_e$, $M^2/M_\mu = 1$ Mev, so there appears to be little chance of measuring the masses of the neutral particles with present day resolving powers.

APPENDIX B

Figures 11 through 16 are representative of the large majority of the photographs obtained. Figures 17, 18, 19, exemplifying decays in the gas, occur more rarely.

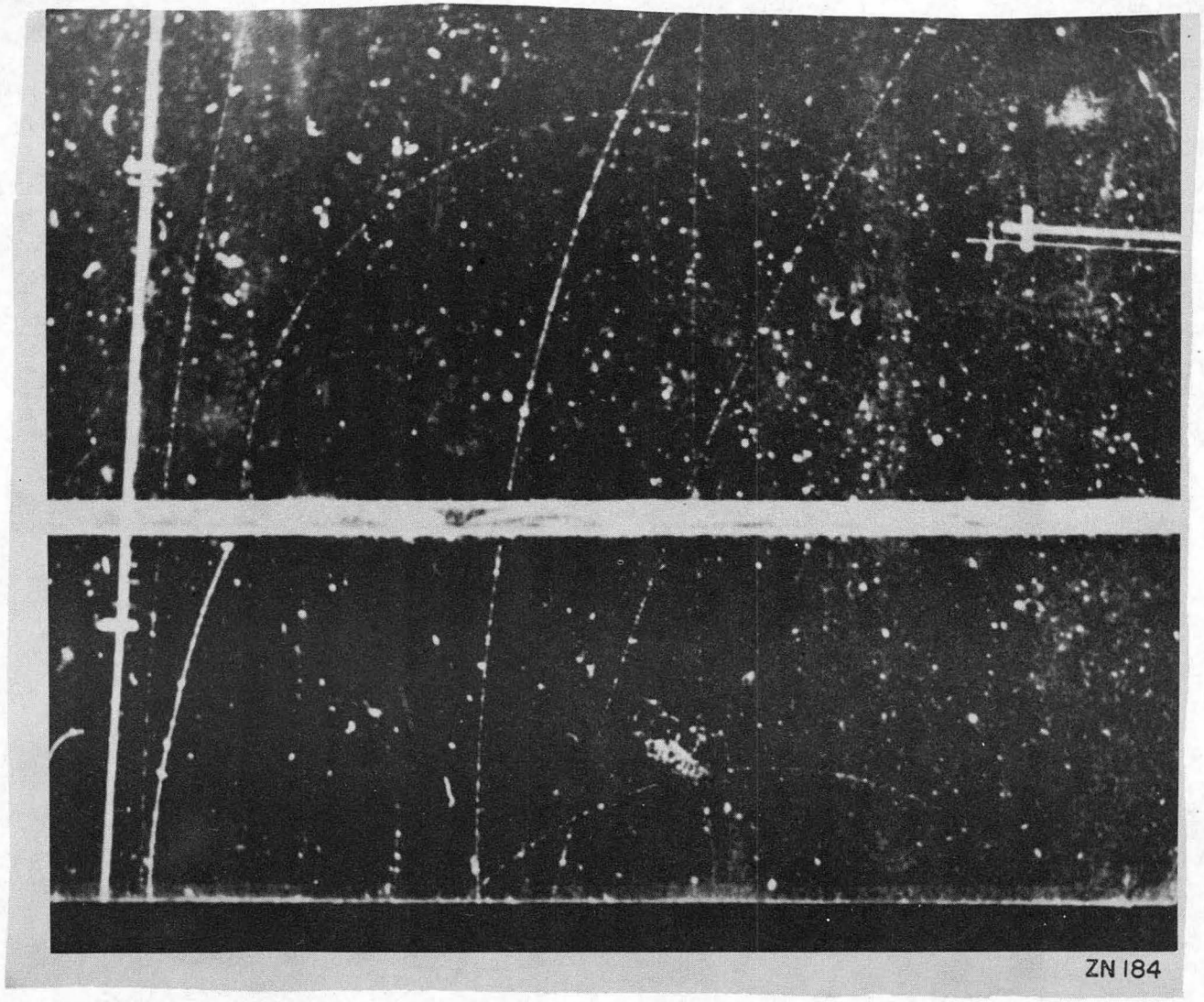

Fig. 11

A typical event, π-μ-β decay occuring in the carbon.

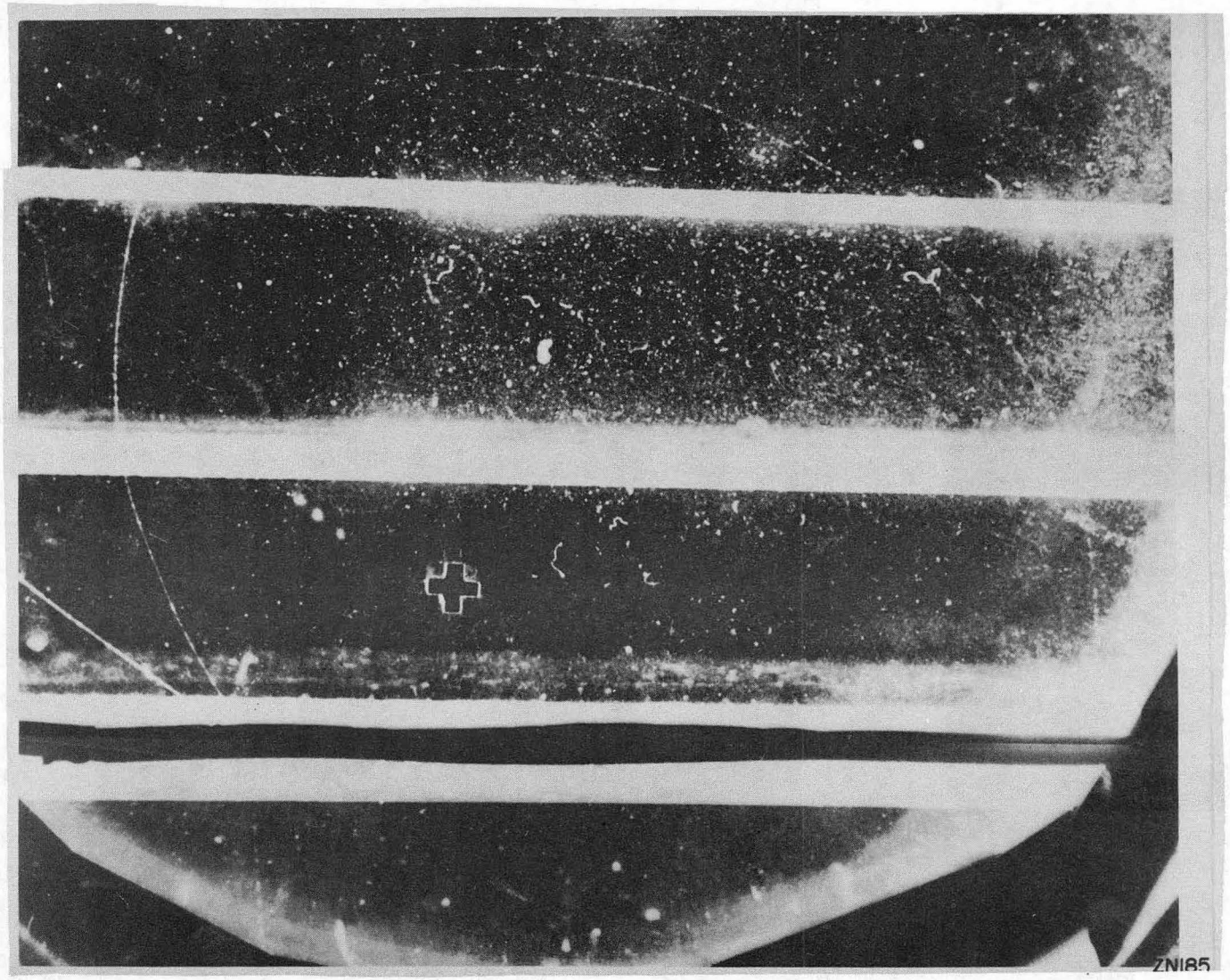

Fig. 12

A typical event. π-μ decay occurs in the carbon, and the positron emerges into the gas.

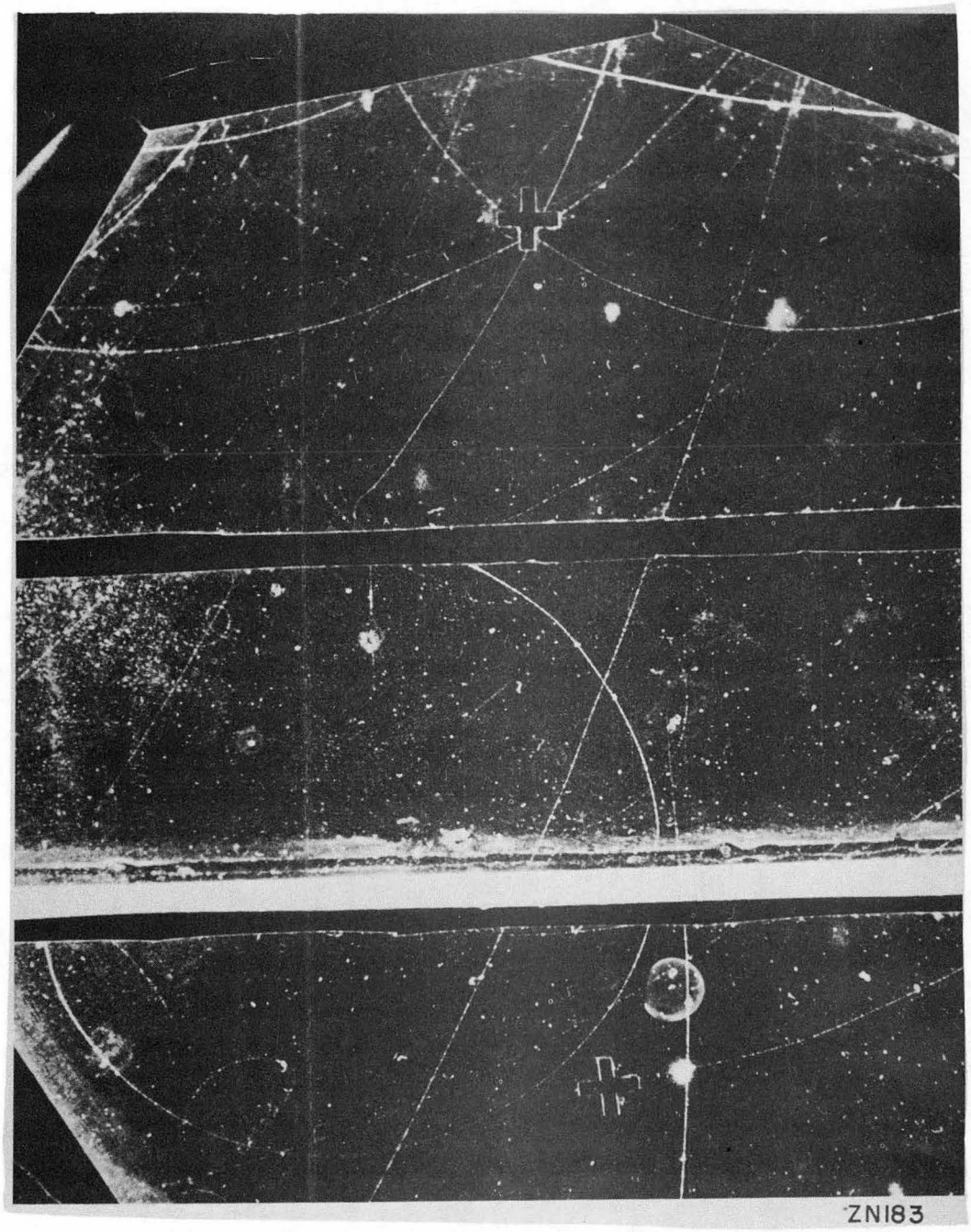

Fig. 13

A typical event. The electron can be seen in the space above the plate.

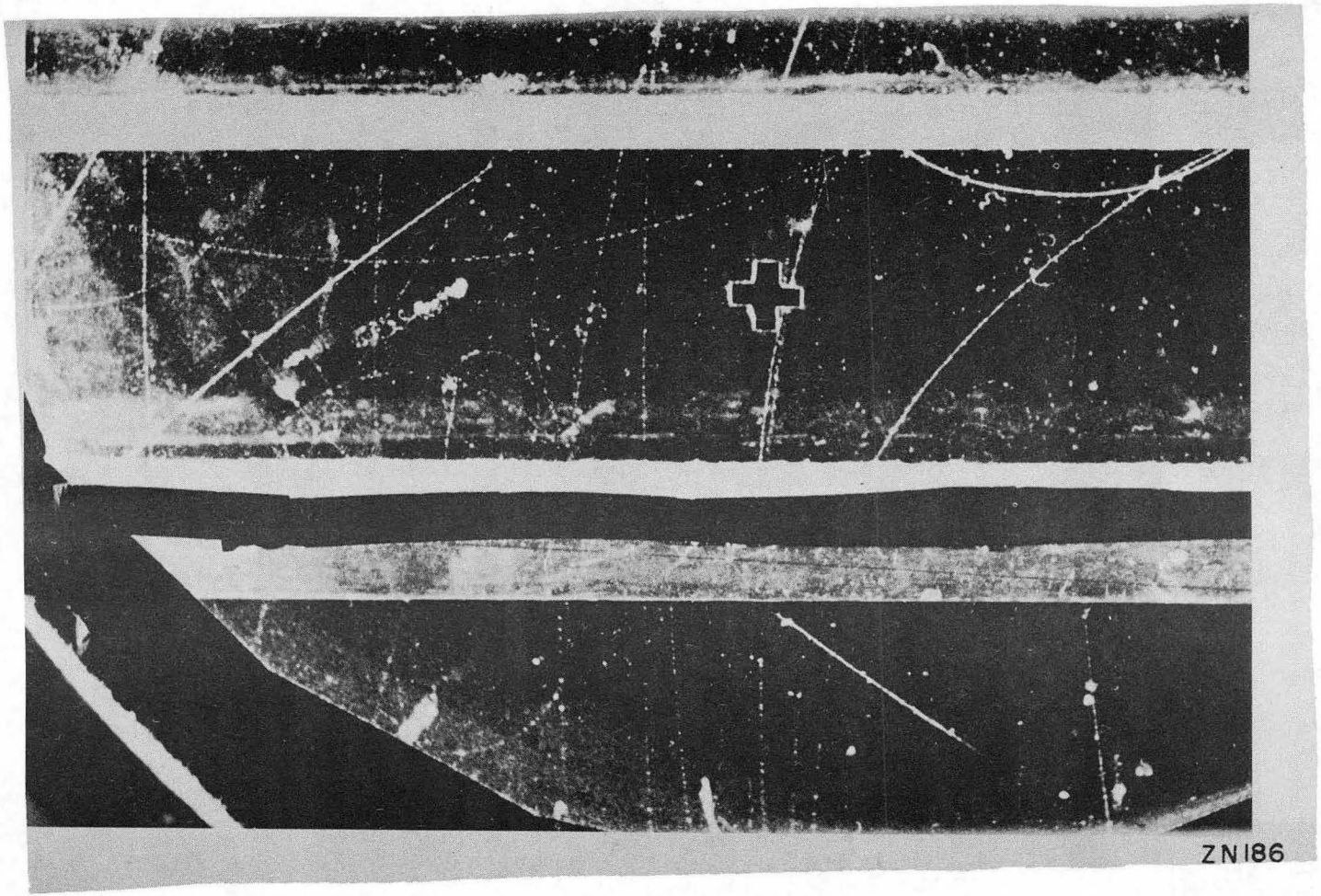

Fig. 14

A π meson scatters before decaying in the upper plate.

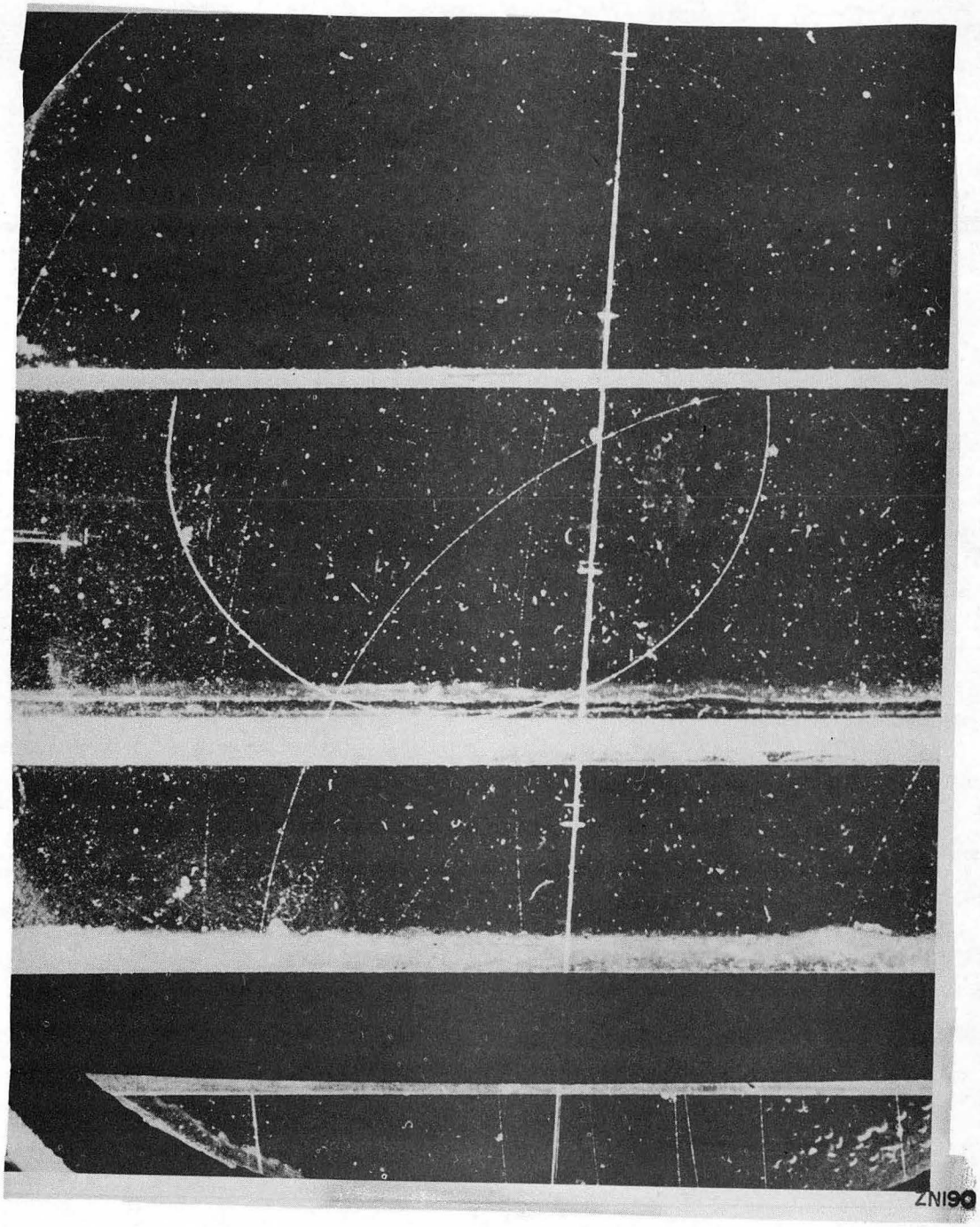

Fig. 15

The π meson either scatters or decays in the plate and the decay positron appears after the second entrance of the plate.

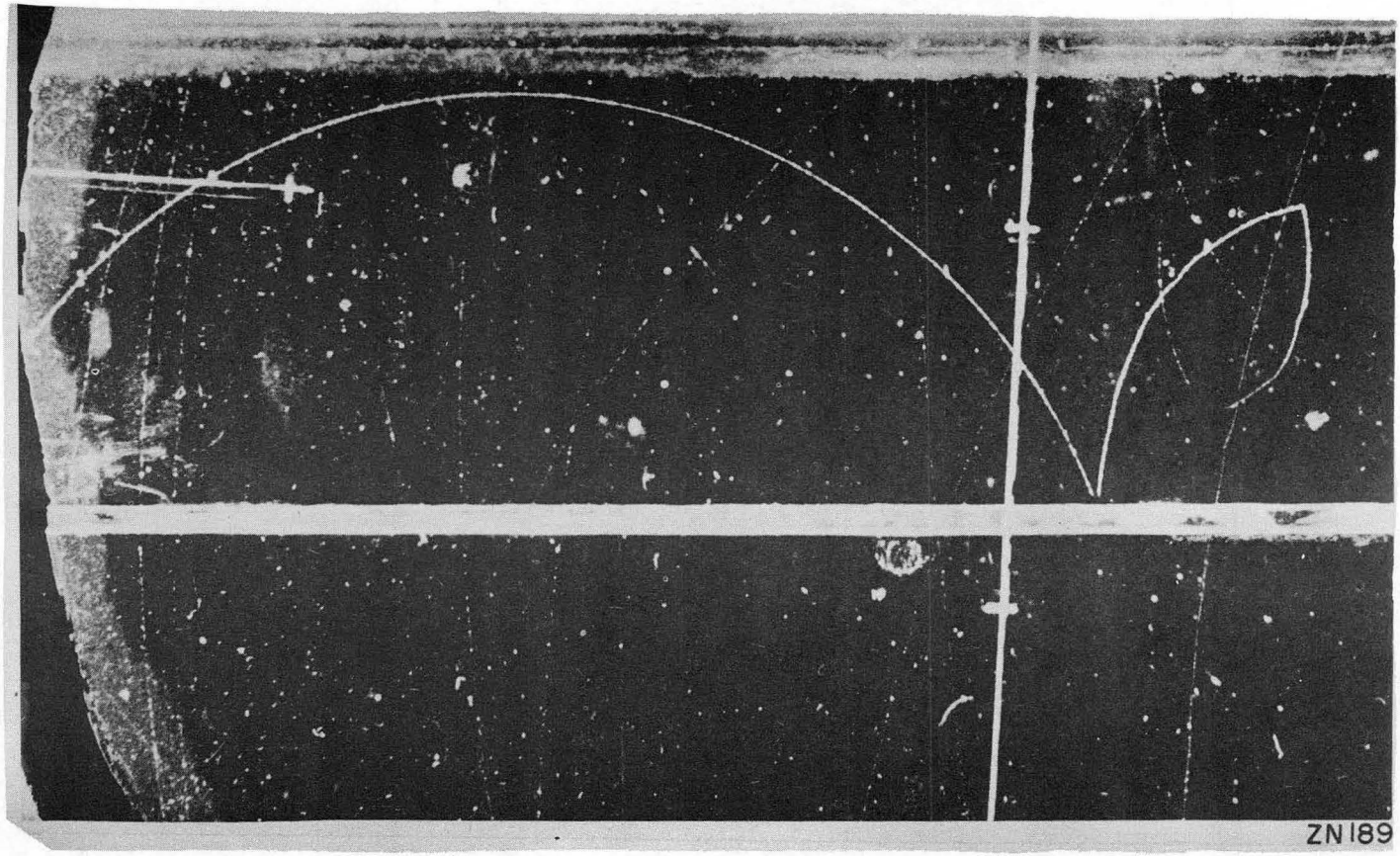

Fig. 16

A π meson scatters in the plate, decays into a μ in the gas. The μ passes out of the lighted region into the bottom of the chamber, decays, and the positron appears in the gas.

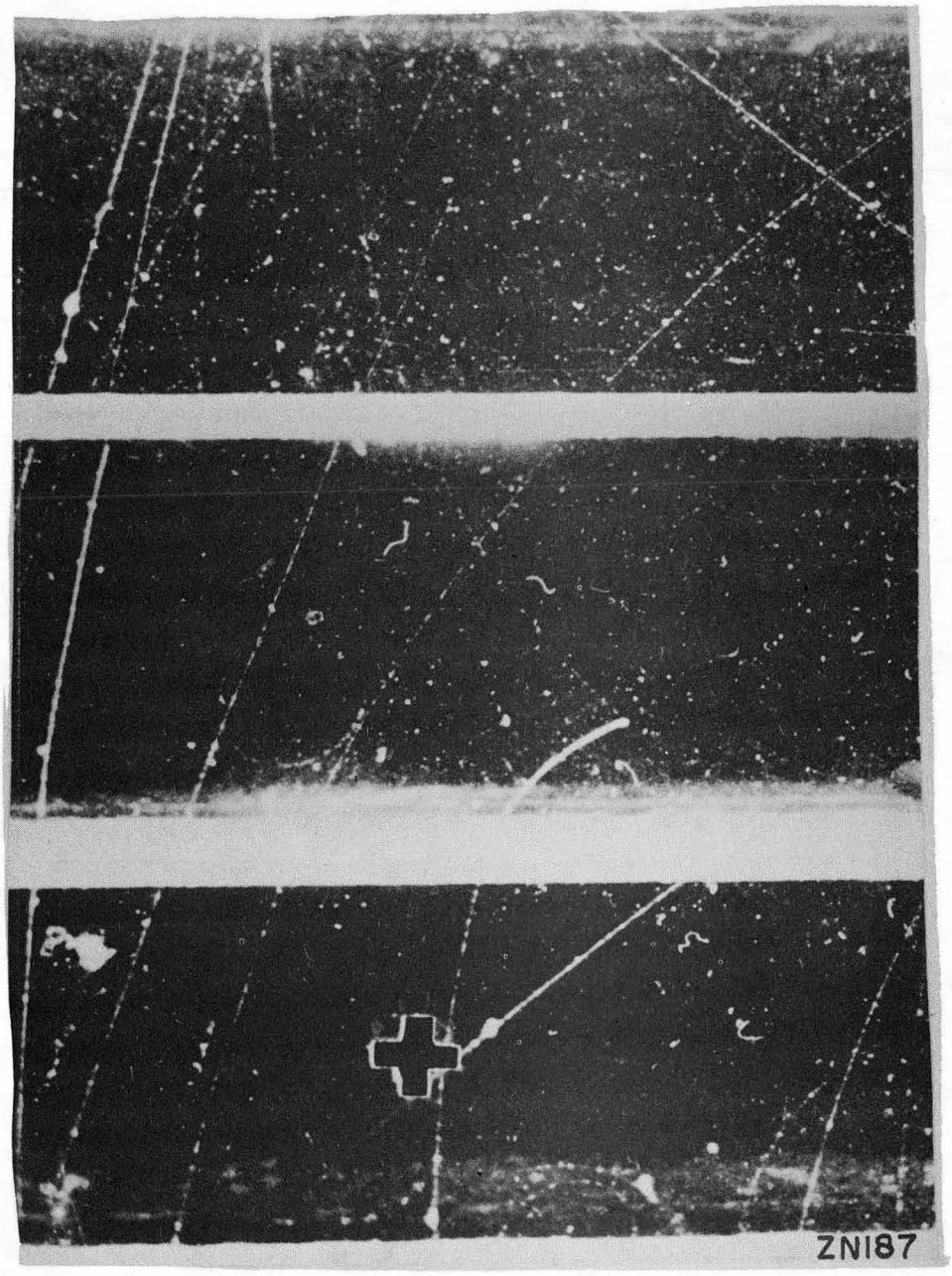

Fig. 17

A μ meson emerges from the plate and decays in the gas.

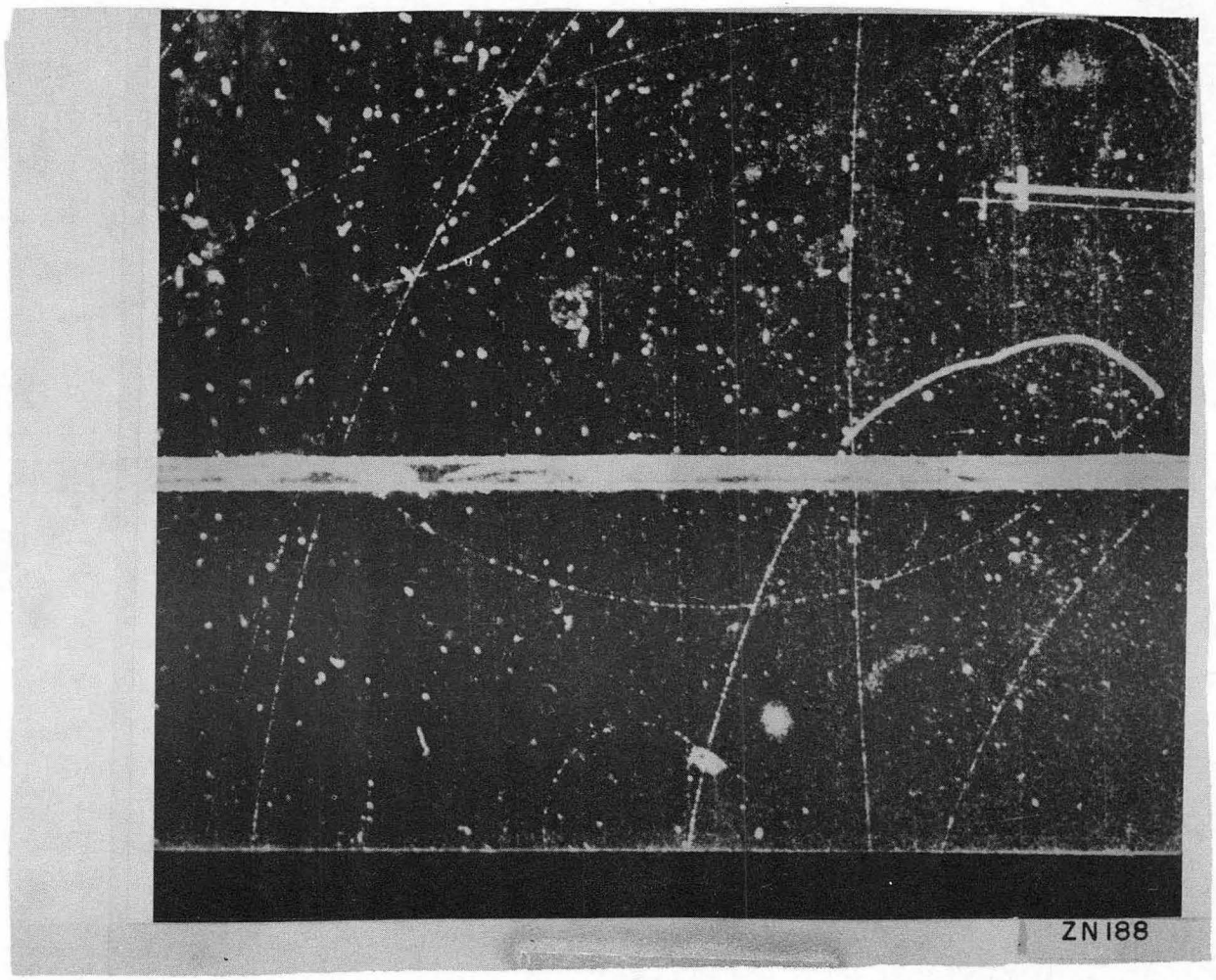

Fig. 18

A μ meson decay in the gas of the cloud chamber.

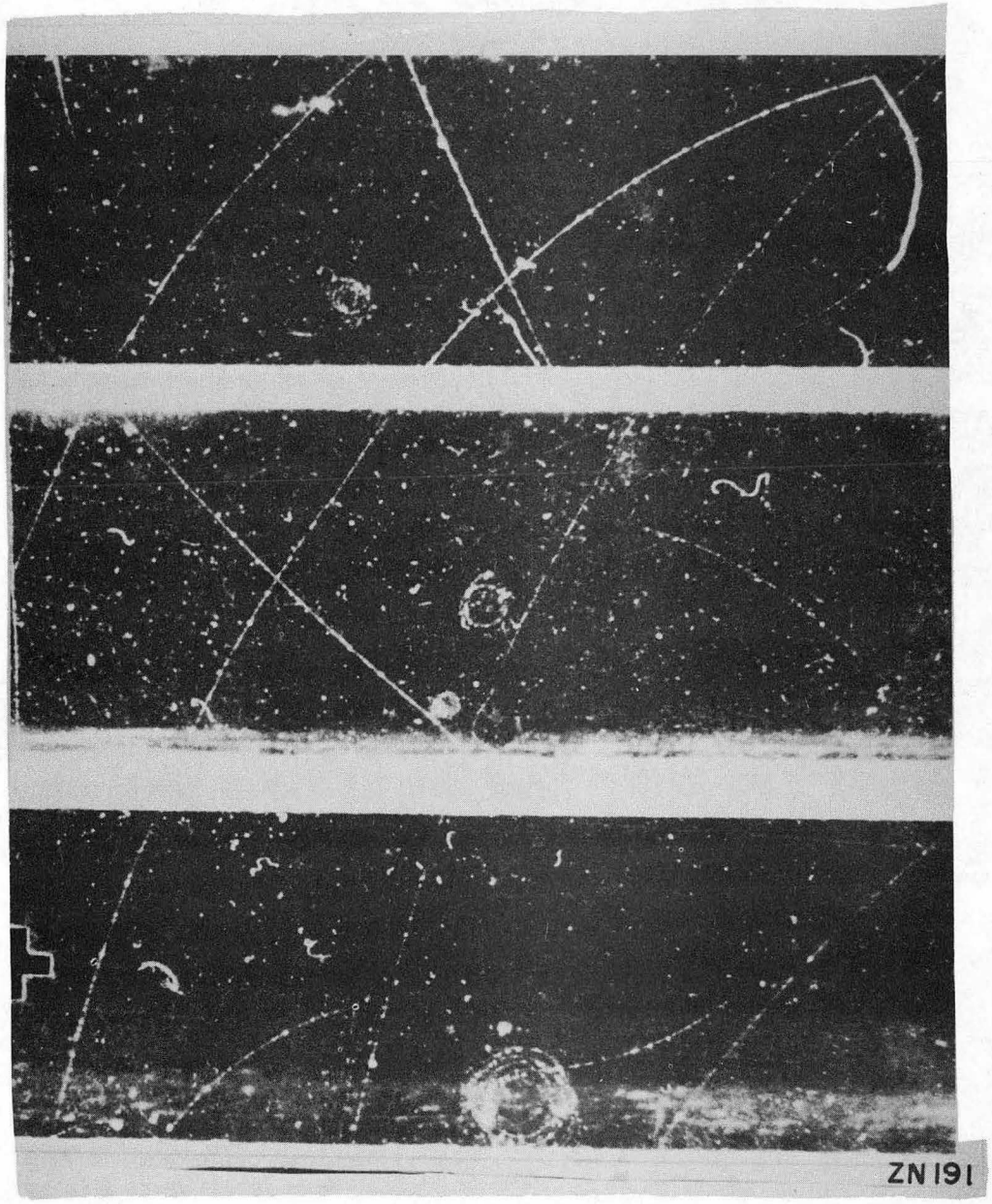

Fig. 19

Here either a μ is scattered and decays in the gas or π-μ and μ-β decays both occur in the gas.